Experiments with Macroscopic Active Matter

Master's thesis in Complex Adaptive Systems

ANGELO DAVID BARONA BALDA

DEPARTMENT OF APPLIED PHYSICS
CHALMERS UNIVERSITY OF TECHNOLOGY
Gothenburg, Sweden 2022
www.chalmers.se

Master's thesis 2022

Experiments with Macroscopic Active Matter

ANGELO DAVID BARONA BALDA

CHALMERS
UNIVERSITY OF TECHNOLOGY

Department of Applied Physics
Division of Soft Matter
Soft Matter Lab
Chalmers University of Technology
Gothenburg, Sweden 2022

Experiments with Macroscopic Active Matter
ANGELO DAVID BARONA BALDA

Supervisor: Aykut Argun, Giovanni Volpe
Examiner: Giovanni Volpe, Department of Physics

Master's Thesis 2022
Department of Applied Physics
Division of Soft Matter
Soft Matter Lab
Chalmers University of Technology
SE-412 96 Gothenburg
Telephone +46 31 772 1000

Cover: Snapshot of active particles rotating a static gear.

Typeset in LaTeX
Printed by Chalmers Reproservice
Gothenburg, Sweden 2022

Experiments with Macroscopic Active Matter ANGELO DAVID BARONA BALDA
Department of Applied Physics
Chalmers University of Technology

Abstract

Active matter research has been very prominent in the last decades. However, this field mostly investigates microscopic particles. For this reason, most of the studies so far rely on pure mathematics or numerical simulations to prove their points. In this project, we select a set of simulations and create macroscopic experimental setups to test the theoretical results. We use small self-propelling robots to emulate microscopic active matter in a large scale. In the end, we demonstrate that these macroscopic experiments are a good approximation of microscopic active systems. Our setups are useful for potential didactic applications.

Keywords: active matter, active particles, robots, HEXBUGS, chirality.

Acknowledgements

First and foremost, I would like to thank my mother, Patricia Balda, for her immense support in making the adventure of this master's degree.
Next, I thank my examiner, Giovanni Volpe, and my supervisor, Aykut Argun. Their support, patience, and contributions were key to complete this project successfully. I also want to thank all the members of the Soft Matter Lab. They have been incredibly welcoming and helpful during this time. And finally, I thank Leonardo Martínez for sharing his photo editing skills at moments when mine were lacking.
Thank you all for your incredible support.

Angelo David Barona Balda, Gothenburg, June, 2022

Contents

List of Figures

1

Introduction

Active matter is a substance or system composed of individual agents that consume energy. These agents use the energy to vibrate, self-propel, or apply force to their surroundings. As a result of the exchange of energy, the entire system phases out of equilibrium. In the non-equilibrium state, we observe emerging collective phenomena among the agents in the system. These phenomena usually involve coordinated activities that the agents could not perform independently.

Most instances of active matter comprise microscopic agents. Some examples are colloids, bacterial baths, and cellular tissues. However, other few examples include macroscopic agents, such as flocks of birds, swarms of insects, and crowds of people.

Currently, much of the ongoing research on active matter focuses on the microscopic level. In practice, studies of microscopic active particles influence developments in fields like biomedicine, pharmaceutics, and nanotechnology [12]. A prominent example the application of active matter science in drug delivery advances.

In 2012, Joseph Wang and Wei Gao explained in their paper [8] the advantages and challenges of using microscopic "shuttles" for drug delivery in the human body. These "shuttles" would contain nanoscopic motors that propel them throughout the blood stream. In this way, these small particles could efficiently transport large amounts of medicine to damaged tissue, like cancer cells.

Although this approach is promising, it creates many challenges. For example, many "shuttles" lack the required force to penetrate some kinds of tissues. Also, the interactions with the blood flow complicates the trajectory of the particles. Nonetheless, this application demonstrates the importance of active matter in current research.

The topic of active matter is also relevant in the theoretical aspect. It helps statistical physicists to test equations and concepts of non-equilibrium physics [2]. Additionally, professors use active matter as a gateway to introduce students into non-equilibrium research. However, it is difficult to intuitively explain the behavior of microscopic particles.

To better visualize these particles, academics frequently use simulations, both in classrooms and in research. There are multiple techniques to numerically simulate an active system. For example, in a 2014 study, Giorgio Volpe, Sylvain Gigan, and

Giovanni Volpe explain how to simulate active matter in different settings [4].

In their paper, they explain how to discretize the mathematical model of Brownian motion for active matter. The model is tested in different environments, where the authors analyzed the multiple trajectories. This is an example of a theoretical experiment that is both didactic and relevant for further research.

For some recent studies, scientists have developed artificial particles, which enable them to experimentally study their dynamics. One case is the experiments performed by Marco Leoni et al., where they fabricated a macroscopic prototype of an active particle [5].

Additionally, they used existing toy robots called **HEXBUGS** as a second type of particle [5]. HEXBUGS are small, self-propelling devices that move by vibrating. Although these robots move autonomously, they have no control over their direction, which results in random patterns of motion.

The authors studied the particles in multiple environments and tracked their behavior. When comparing the behavior to the theoretical model of active motion, the authors observed that both were similar. Although the macroscopic case is subject to friction and inertia, it expands the possibilities of active matter research.

In this project we combine the theoretical and experimental aspects of active matter research. We use the HEXBUGS to replicate simulations performed in previous research papers. The objective is to demonstrate that macroscopic particles, like the HEXBUGS, resemble active particles in multiple heterogeneous environments.

We also aim to keep these demonstrations didactic, understandable and easy to reproduce. In this way, the experiments will help to improve the learning experience of active matter and non-equilibrium systems in general.

2

Theory

Although this project is mostly experimental, it is based on theoretical background described on other simulation studies. This chapter explains the concepts that are tested in this thesis project.

2.1 Brownian Motion

One of the key concepts in this project is Brownian motion. **Brownian motion** ($B(t)$) is a stochastic process that describes the random walk of a particle in a medium. Mathematically, $B(t)$ has the following characteristics:

- $B(t)$ is continuous in time t.
- $B(t)$ always starts at 0 ($B(0) = 0$).
- An increment $B(t+s)-B(s)$ always follows a normal distribution. This means that the average difference between steps is 0, with standard deviation 1.
- $B(t)$ has independent increments. This means that the magnitude of an increment at time $t = T$ is not affected by any increments at times $t < T$.

In physics, Brownian motion is used to describe the movement of microscopic particles in media like air and water. As a result of their random walks, the particles diffuse along their medium as time progresses.

2.2 Active Brownian Motion

As explained in the previous section, agents present in active matter use energy to self-propel. In this context, these agents are called **active particles** [13].

Microscopic active particles, such as bacteria, protozoa, or viruses, commonly live in fluids that are filled with other microorganisms and molecules, with which they constantly collide. These collisions erratically deviate the trajectories of active particles, resulting in a random walk. This stochastic process is called **active Brownian motion** [6].

The basic mathematical model to define active Brownian motion for a single particle is [4]:

$$\frac{d}{dt}\phi(t) = \Omega + \sqrt{2D_R}W_\phi, \tag{2.1}$$

$$\frac{d}{dt}x(t) = v\cos\phi(t) + \sqrt{2D_T}W_x, \tag{2.2}$$

$$\frac{d}{dt}y(t) = v\sin\phi(t) + \sqrt{2D_T}W_y, \tag{2.3}$$

where:

- x and y are the position coordinates of the particle.
- ϕ is the orientation of the particle with respect to the x axis.
- Ω is the angular velocity of the particle.
- v is the linear velocity of the particle.
- D_T and D_R are the translational and rotational diffusion coefficient of the particle respectively.
- W_ϕ, W_x, W_y are independent Brownian processes with a mean of 0 and a variance of 1.

When $\Omega = 0$, the particle mainly displays translational diffusion. Therefore, the diffusion is very similar to that described by standard Brownian motion in terms of direction.

When $\Omega \neq 0$, we call the particle *chiral*. In this case, the particle experiences a torque due to its interaction with the medium. As a result, the particle also displays angular motion and rotational diffusion.

The sign of Ω defines the orientation of the rotation of the particle. The orientation can be either clockwise or counter-clockwise.

3

Methods, Materials, and Techniques

This chapter details the materials that we used for the experimental setup. It also explains the techniques that we applied for the data analysis.

3.1 HEXBUGS as Active Particles

The HEXBUG nano® is a small toy robot manufactured by Innovation First, Inc. FIG 3.1 is a picture of this model.

Figure 3.1: Sample of a HEXBUG nano®. Image Obtained from [14]

This robot requires an LR44 battery, which powers up its internal motor. The motor produces vibrations that propel the robot forward thanks to the shape and structure of its legs.

Every HEXBUG nano® has six legs on each of its lateral sides. The legs are angled and rubbery, as shown if FIG 3.1. This causes the mechanical energy of the

vibrations to move the robot forward.

The behavior of the HEXBUGS matches with the definition of active matter that we provided in chapter 1. For this reason, we use these robots to emulate active particles in this paper.

3.2 Cardboard Boxes as Boundaries

The experiments in this project require physical boundaries to enclose the area of the analysis. We created our own boundaries by using scraps of cardboard boxes. We assembled two set boundaries:

- A set of bounding walls of 44 × 44 cm, shown in FIG. 3.2.
- A set of bounding walls of 88 × 44 cm, shown in FIG. 3.3.

Figure 3.2: Bounding Walls, 44 × 44 cm

To build the build the boundary:

1. We cut pieces of cardboard of the appropriate length.
2. We formed a squared boundary and a rectangular boundary with the pieces of cardboard and held them together using tape.
3. We painted the boundaries using black aerosol.
4. We covered the corners using black paper, making the corners rounded instead of rectangular.

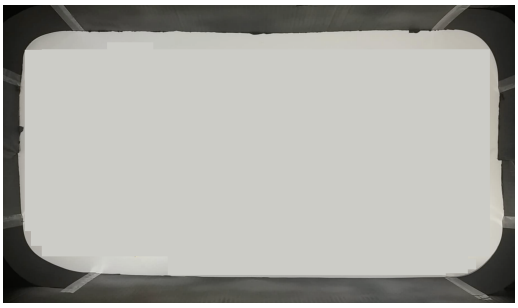

Figure 3.3: Bounding Walls, 88 × 44 cm

We make the corners as round as possible to prevent HEXBUGS from being stuck in unnecessary places.

3.3 3D Printed Shapes as Obstacles

For various experiments in this project, we needed to create obstacles to modify the environment. Since we required unconventional shapes, we 3D printed the obstacles for simplicity. FIG. 3.4 shows some of the objects we used.

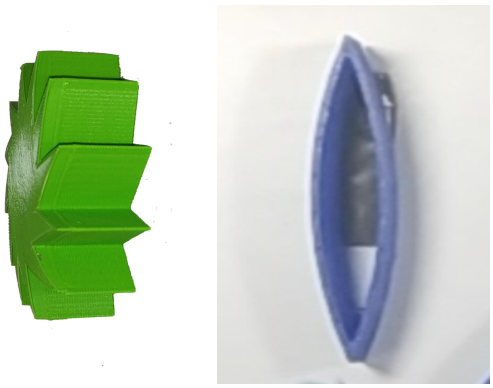

Figure 3.4: Sample of 3D-Printed Objects Used in the Project

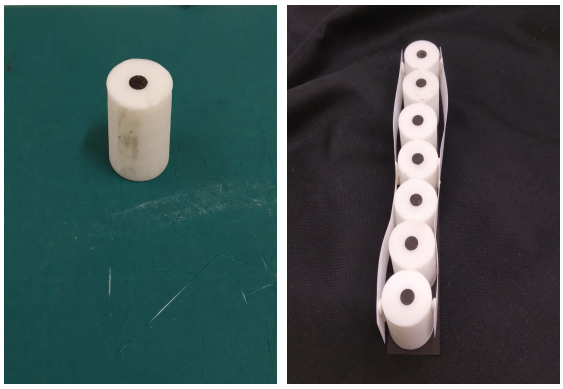

Figure 3.5: Small 3D-Printed Cylinders Used to Create Multiple Shapes

FIG. 3.5 illustrates small 3D-printed cylinders (radius=1.9 cm, height=2 cm). We glued together multiple of these cylinders to create larger obstacles. In this way we could modify the shape and dimensions of the obstacles as necessary.

3.4 Cellphone Camera as Filming Equipment

To exhaustively analyze the behavior of the HEXBUGS, we recorded every experiment that we performed. Considering that the experiments must be easily replicable, we chose a cellphone camera for filming. We used the camera of a Xiaomi Redmi S2, a 12 MP + 5 MP dual camera [15]. FIG. 3.6 shows a picture of the cellphone.

Figure 3.6: Xiaomi Redmi S2

3.5 OpenCV as an Analysis Tool

To track and analyze the trajectories of the HEXBUGS, we used OpenCV. OpenCV is a computer vision library that is available for Python and C++ [16]. OpenCV has several features relevant for our analysis, such as:

- Image Processing
- Video Analysis
- Video Input/Output

The Python API for OpenCV enables us to call functions from the library using Python. In conjunction, we used libraries like NumPy and matplotlib to compute and plot the data collected with OpenCV.

4

Experiments: Background, Results, and Discussion

This chapter explains how we performed the selected experiments and the steps to reproduce them. It also discusses the results of said experiments.

4.1 Single Active Brownian Particle

In this experiment, we show *non-chiral* active Brownian motion ($\Omega = 0$). The objective is to reproduce the behavior that the mathematical model displays in simulations. As a reference, we use the results obtained by Clemens Bechinger et al. in their research from 2016.

In their research paper, the authors simulate the trajectories of active Brownian particles using equations 2.1 to 2.3. They show that the particles can traverse in a straight line only for a certain distance before randomly changing directions. This distance is called the *persistence length* [9]. It is defined as follows:

$$L = \frac{v}{D_R} \tag{4.1}$$

where v is the velocity of the particle and D_R is the rotational diffusion coefficient. FIG. 4.1 shows a depiction of sample trajectories of non-chiral active Brownian motion.

Furthermore, the authors propose a strategy to illustrate the concept of persistence length in active Brownian motion. They suggest to analyze the average particle trajectory starting from the coordinate $x(0) = y(0) = 0$ and with orientation $\phi(0) = 0$. The resulting average must be a line along the x-direction, which is defined as [9]:

$$\langle x(t) \rangle = \frac{v}{D_R} \left[1 - e^{-D_R t} \right] \tag{4.2}$$

Figure 4.1: Diagram of a Non-Chiral Active Brownian Particle and Some Sample Trajectories. Image Obtained From [9]. **a** is a depiction of an active particle. The following panes show the resulting non-chiral trajectories with velocities **b** $v = 0$ μm/s, **c** $v = 1$ μm/s, **d** $v = 2$ μm/s, and **e** $v = 3$ μm/s

This experiment focuses on reproducing this strategy. To do that, we set up the experiment as follows:

1. We used the boundary shown in FIG. 3.2 to confine an area on a smooth table.
2. We stuck a bright-colored tag on a HEXBUG for tracking purposes.
3. We put the HEXBUG within the boundary and allowed it to move freely.

Using OpenCV we tracked the motion of the HEXBUG. FIG. 4.2b shows snapshots of the trajectory. As expected, the motion is predominantly straight until the robot collides with a wall, when it randomly changes direction.

Next, we analyzed the recorded trajectory to demonstrate that the HEXBUG behaves as an active Brownian particle. To do so, we characterized the motion as follows:

1. We split the trajectory into smaller parts that represent the motion between collisions.
2. We translated and rotated each part of the trajectory so that all of them start at $x = 0$, $y = 0$, and $\phi = 0$.
3. We computed the mean of all the parts of the trajectory.

As shown in FIG. 4.2c, the mean trajectory is a quasi-straight line along $y = 0$. This is expected because as it is consistent with the statement in the article by Bechinger et al. The average is not perfectly straight because the trajectory of the robot in between collisions is slightly deviated to one side. This is probably due to fabrication imperfections. Nonetheless, this proves that HEXBUGS can emulate non-chiral active Brownian particles, with an angular velocity $\Omega \approx 0$.

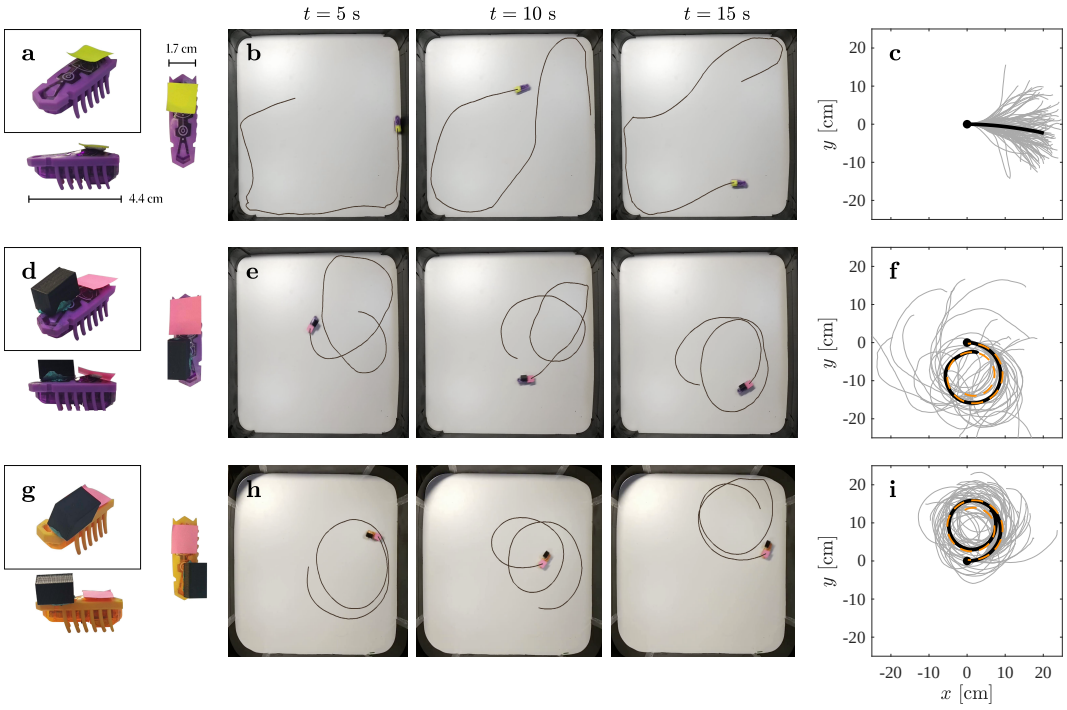

Figure 4.2: Sample trajectories of regular and chiral active Brownian motion. **a** shows a HEXBUG with no modifications. **b** shows a snapshot of active Brownian trajectories at $t = 5s$, $t = 10s$, and $t = 15s$. **c** shows a sample of 91 trajectories and the mean of these trajectories (thick black line). **d** shows a HEXBUG with an extra weight on its top-right side. **e** shows a snapshot of chiral *dextrogyre* Brownian trajectories at $t = 5s$, $t = 10s$, and $t = 15s$. **f** shows a sample of 22 chiral *dextrogyre* trajectories and the mean of these trajectories (thick black line). This mean is also fitted to a *spira mirabilis* (dashed orange line). **g** shows a HEXBUG with an extra weight on its top-left side. **h** shows a snapshot of chiral *levogyre* Brownian trajectories at $t = 5s$, $t = 10s$, and $t = 15s$. **i** shows a sample of 29 chiral *levogyre* trajectories and the mean of these trajectories (thick black line). This mean is also fitted to a *spira mirabilis* (dashed orange line).

4.2 Chiral Active Brownian Particle

In the following part of the experiment, we show *chiral* active Brownian motion ($\Omega \neq 0$). As in thhe previous experiment, the objective is to reproduce the simulations based on equations 2.1-2.3. As a reference, we use the results in the paper by Mijalkov and Volpe (2013).

In their research, they show how, in homogenous environments, particles with non-zero angular velocity show circular trajectories. Furthermore, the average these trajectories forms a logarithmic spiral (*spira mirabilis*). FIG. 4.3 shows a diagram that shows sample trajectories of chiral active Brownian motion.

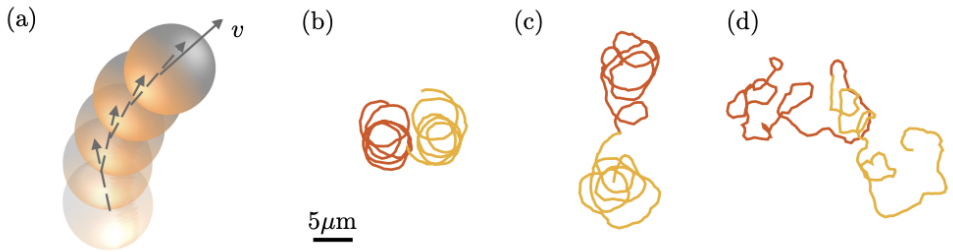

Figure 4.3: Diagram of a Chiral Active Brownian Particle and Some Sample Trajectories. Image Obtained From [9]. **a** is a depiction of an active particle. The following panes show the resulting chiral trajectories with velocities $v = 1$ μm/s and $\Omega = 10$ rad/s. The radii of the particle is **b** 1000 nm, **c** 500 nm, and **d** 250 nm

The set up of the experiment is the same as in the previous section. However, to induce chirality on the HEXBUG, we glued a small 3D-printed parallelepiped on top of the robot. This object exerts weight on the robot and deviates the trajectory in a certain direction.

FIG. 4.2d and 4.2g show the two placements of the object. We placed the object on the top-right side to generate clockwise motion (dextrogyre chirality), and on the top-left side to generate counter-clockwise motion (levogyre chirality).

To track and analyze the trajectories, we proceeded as described in the previous section. As shown in FIG. 4.2e and 4.2h, the motion is effectively deviated in the intended directions.

FIG. 4.2f and 4.2i show the mean trajectory for the dextrogyre and levogyre cases respectively. We observe that in the first case, the mean trajectory is a spiral-shaped curve oriented to the right, while in the second case, the curve is oriented to the left.

This is expected because these trajectories are consistent with those in the simula-

tions by Mijalkov and Volpe. Therefore, we can also characterize the chiral motion as a *spira mirabilis*.

The cartesian coordinates of a *spira mirabilis* are defined by the following equations:

$$x(\phi) = ce^{a\phi}\cos\phi, \quad y(\phi) = ce^{a\phi}\sin\phi \tag{4.3}$$

where $c > 0$ and $a \neq 0$ are constants. By testing different parameters, we found the equations that fit the trajectories in figures 4.2f and 4.2i:

$$x(\phi) = 1.5 - 1.9e^{0.05\phi}\cos\phi, \quad y(\phi) = \pm 8.7 + 1.9e^{0.05\phi}\sin\phi \tag{4.4}$$

where $\phi \in [20, 30]$ and the sign of y depends on the chirality of the particle. The orange line in figures 4.2f and 4.2i represent the plot of equation 4.4. As expected, it theoretical trajectories are very similar to the experimental results.

4.3 Interaction Between Particles and Obstacles

In this section we show how non-chiral active particles interact with their surroundings. In a homogeneous environment, the motion trajectory of the particles is unpredictable. However, by modifying the environment correctly, it is possible to organize the particles so they can perform a specific action [1].

A strategy to order the system is introducing obstacles. Nonetheless, obstacles with symmetric shapes do not notably affect the behavior of the particles. This occurs due to the symmetric nature of Brownian motion [1]. To break the symmetry of the system and induce self-organization, we must introduce asymmetric obstacles.

In the following experiments, we use two type of objects to rectify the trajectories of active particles: rods and gears. We record the behaviors when the objects are loose and when they are fixed to the surface.

4.3.1 Interaction with Loose Rods

The objective of this experiment is to observe how the particles displace specific types of rods. The set up is based in a paper by Angelani and Di Leonardo (2010) [10]. In their paper, they simulated a bath of self-propelled bacteria, where they immersed a large V-shaped "shuttle". FIG. 4.4 shows a depiction of the shuttle.

Their simulations showed that, due to its asymmetric shape, the V-shaped shuttle trapped and aligned the particles to a specific direction. This caused the object to be propelled in the direction of the alignment.

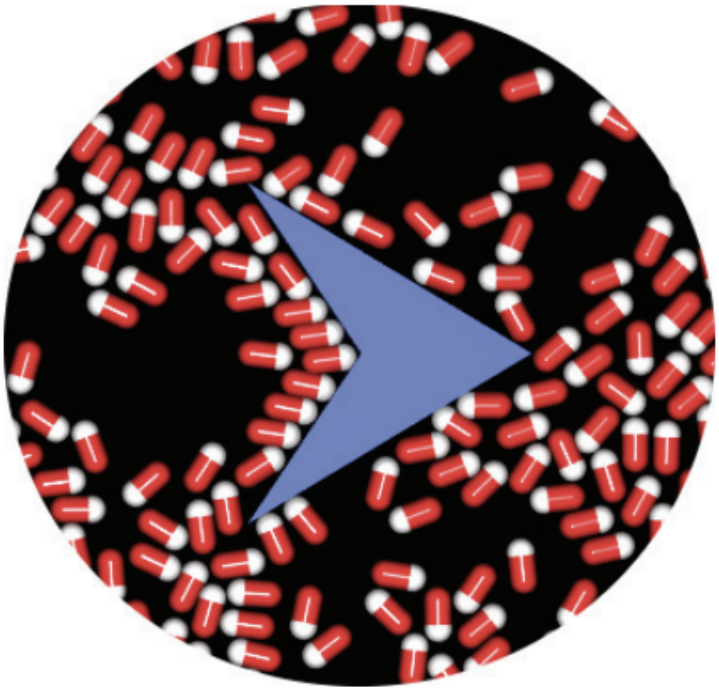

Figure 4.4: Depiction of a Micro-Shuttle. Image Obtained From [10].

Although in the original experiment, the authors used more than 1000 particles, for this recreation we used only **14** unmodified HEXBUGS. This is because of limitations of space and simplicity. Additionally we assembled our version of the shuttles using the small 3D-printnted cylinders shown in FIG. 3.5. We created the following objects:

- An V-shaped asymmetric rod
- A regular symmetric rod

The V-shaped rod emulates the "shuttle" used in the paper by Angelani and Di Leonardo. The regular rod is used for a control experiment. We set up the experiments as follows:

1. We used the boundary shown in FIG. 3.2 to confine an area on a smooth table.
2. We stuck a bright-colored tag on the selected rod.
3. We placed the rod in the center of the confined area.
4. We homogeneously distributed the 14 HEXBUGS within the boundary and allowed them to move freely.

We ran the experiment independently with each of the rods. FIG. 4.6a and 4.6c show snapshots of the trajectories for the V-shaped and the regular rod respectively.

We observe that the V-shaped rod was displaced further that its counterpart. This is expected because the concave shape of the rod rectifies the motion of the HEXBUGS and traps them in its corner. This results in the directed propulsion of the rod [**?**].

Figures 4.6b and d show the cummulative displacement $d(t)$ the V-shaped and the regular rod respectively. The graphs illustrate that the displacement of the V-shaped rod is almost 4 times larger that the regular rod.

4.3.2 Interaction with Fixed Rods

In this part of the experiment, the objective is to use rods as obstacles to trap the particles in one side of the confined area. We aimed to reproduce the results in the papers by Volpe et al. [4] and Wan et al. [7] In their simulations, they used asymmetric barriers to rectify the motion of particles and trap them.

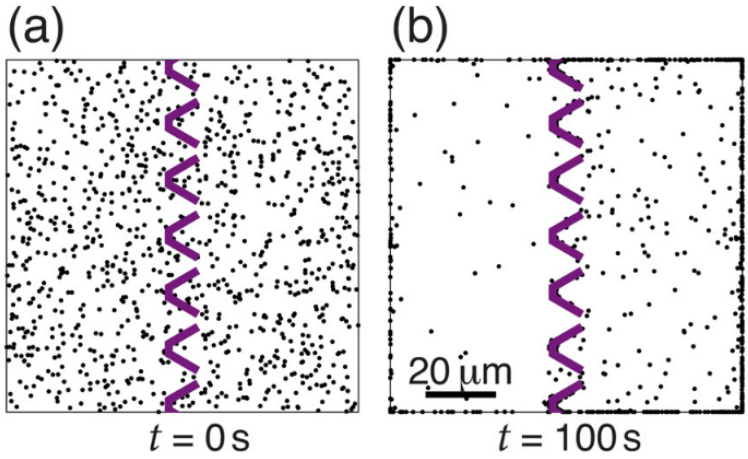

Figure 4.5: Simulated Asymmetric Barriers. Image Obtained From [4]. **a** and **b** show the distribution of the particles at $t = 0$ s and $t = 100$ s respectively.

For this part, we created smaller versions of the rods in experiment 4.3.1 and repurposed them as barriers:

- 3 V-shaped asymmetric barriers
- 3 Regular symmetric barriers

The rods are made up of the same 3D printed cylinders as the rods in 4.3.1.

As in 4.3.1, we also used 14 HEXBUGS. We set up the experiment as follows:

1. We used the boundary shown in FIG. 3.2 to confine an area on a smooth table.
2. We placed the barriers in the horizontal center of the area, with a vertical separation of 2 cm.
3. We stuck a bright-colored tag on each of the 14 HEXBUGS.
4. We homogeneously distributed the HEXBUGS within the boundary and allowed them to move freely.

We ran the experiment independently with each type of barrier. FIG. 4.6e and 4.6g show snapshots of the distribution of the HEXBUGS affected by the L-shaped and regular barriers.

As shown, the V-shaped barriers effectively trap the particles in the left side of the confined area. This is expected because the concave shape of the barrier rectifies the motion of the HEXBUGS and either (a) makes them turn around or (b) traps them in its corner.

Using OpenCV, we tracked the positions of the HEXBUGS during the experiment. FIG. 4.6f and 4.6h show the percentage of particles on the left side of the area with V-shaped and regular barriers respectively.

In the case of V-shaped barriers, we observe that the distribution is homogeneous ($\sim 50\%$) at $t = 0$. As t increases, the percentage of particles increases up to $\sim 90\%$ on the left side. In contrast, the case of regular barriers shows that the percentage remains around 50% throughout the entire run.

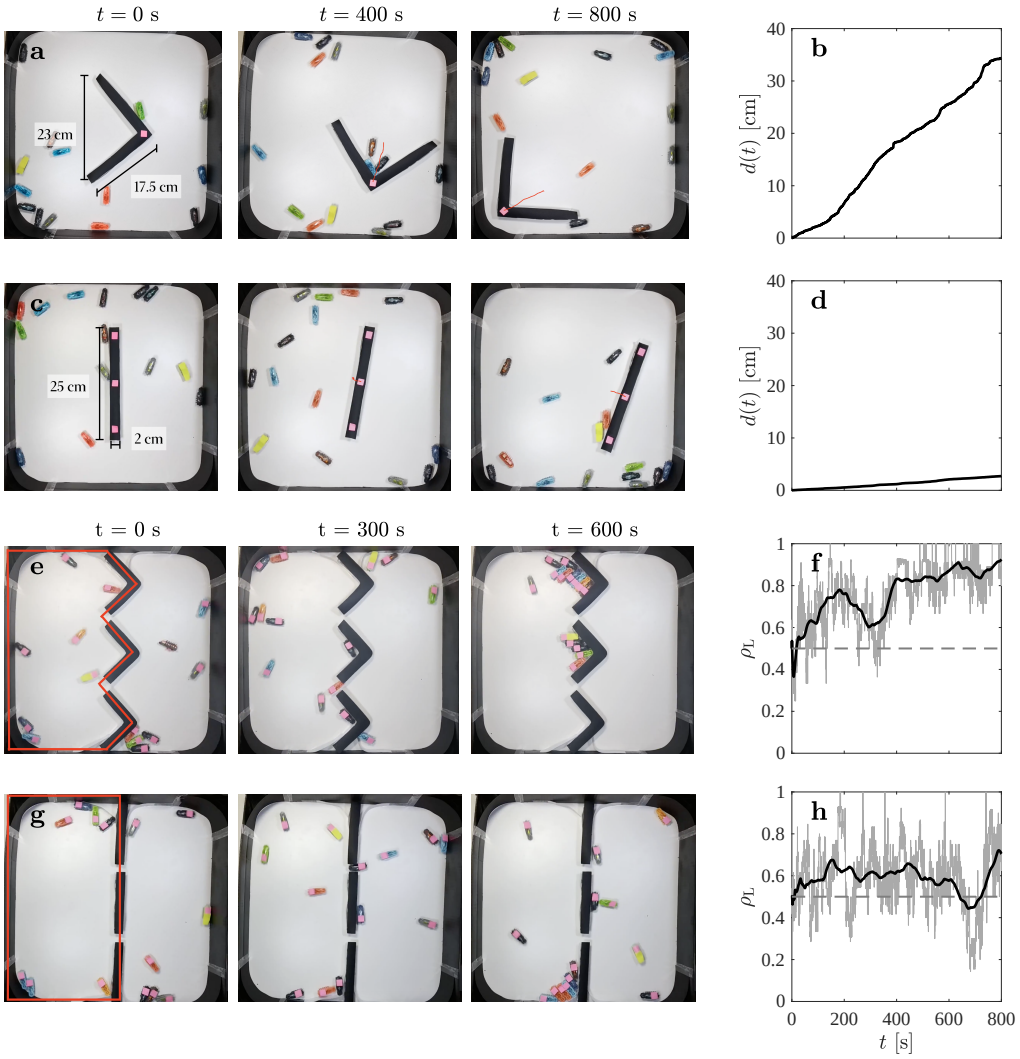

Figure 4.6: Effects of asymmetric and symmetric obstacles on active Brownian motion. **a** and **c** show snapshots of active Brownian particles translating an *asymmetric* and a *symmetric* object on a plane. The pictures illustrate how the particles displace the asymmetric object farther than the symmetric one. **b** and **d** show plots of the displacement $d(t)$ varying in time. **e** and **g** show snapshots of fixed *asymmetric* and *symmetric* obstacles influencing the distribution of the particles on the plane. The pictures illustrate how the asymmetric obstacles affect the distribution more than the symmetric counterpart. **f** and **h** show the how the percentage of particles on the left side of the plane (enclosed in a red perimeter) changes in time. The gray line is the frame-by-frame value. The black line is a smoothed version created by calculating the moving average with a span of 10% of the data points.

4.3.3 Interaction with Loose Gears

This experiment focuses on the interaction of between the particles and asymmetric gears. In this set up, we refer as gears to small disk-shaped objects with several saw teeth. we used two types of 3D-printed gears, gear A and gear B. The only difference between the two gears is the orientation of their teeth. Both gears are shown in FIG. 4.7a and 4.7b.

The objective is to reproduce the behaviors observed in the study by Di Leonardo and Angelani (2009) [1]. In their paper, they immersed different types of gears into a bath of self-propelling bacteria. They showed how the particles became trapped in the corners of the teeth in the gears. When trapped, the propelling force of the bacteria caused the gears to rotate.

As in the previous section, we also used 14 HEXBUGS. We set up the experiment as follows:

1. We used the boundary shown in FIG. 3.2 to confine an area on a smooth table.
2. We stuck two bright-colored tags on the selected gear: one on the center and one on a tooth.
3. We placed the gear in the center of the area.
4. We homogeneously distributed the HEXBUGS within the boundary and allowed them to move freely.

We ran the experiment independently for both of the gears. FIG. 4.7a and 4.7c show snapshots of the trajectories of gears A and B respectively.

In the figures, we observe that the HEXBUGS effectively displace the gears within the area. This happens because, as occurs with the V-shaped rods, the teeth of the gears create concave corners that trap the robots, which causes directed propulsion.

However, the gears have multiple teeth. Therefore, HEXBUGS can get trapped in multiple sides of the gears at the same time. Furthermore, as all the teeth of a gear are in the same orientation, the robots get aligned in the same direction. This causes the gear to rotate in a specific direction.

We measured the rotation of the gear by using OpenCV to track the position of the marked tooth with respect to the center. In FIG. 4.7b and 4.7d show a plot of the cumulative rotational angle of gears A and B respectively.

While the cumulative angle of gear A consistently increases, the angle of gear B decreases. This means that the HEXBUGS cause them to rotate in opposite directions, which is expected because of the orientation of the teeth.

4.3.4 Interaction with Fixed Gears

For this experiment, we continue using gears A and B. The objective is to study the motion of the gears when they are fixed to the surface. To achieve this, we glued a metallic nut to the center of the confined area. As the bottom of the gears is hollow, we could put the gear on top of the nut. FIG. 4.7g displays this set up.

The rest of the set up, as well as the tracking and analysis processes, were the same as those described in the previous section. FIG. 4.7h and 4.7j show snapshots of the motion of gears A and B. FIG. 4.7i and 4.7k show a plot of the cumulative rotational angle of gears A and B respectively.

As expected, the plotted results of this experiment are similar to those of the previous experiment. However, we observe that the gears rotate faster when they are fixed. This happens because fixed gears trap the robots more easily into their concave corners. Also, with fixated gears, the force applied by the HEXBUG is fully applied to a torque and not to linear forces.

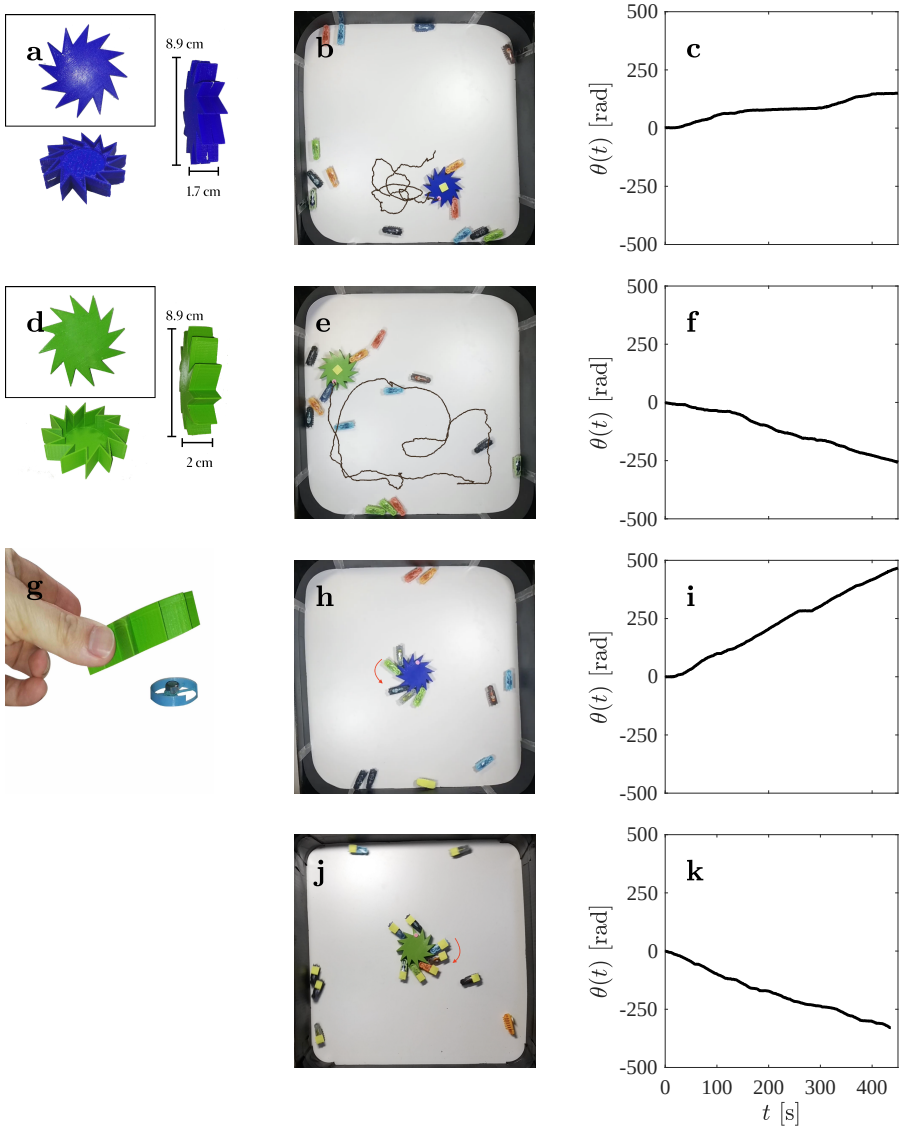

Figure 4.7: Analysis of rotational and translational motion of gears propelled by active Brownian particles. **a** shows a picture of gear A. **d** shows a picture of gear B. **b** and **e** show snapshots of the trajectory of two gears A and B respectively. **c** and **f** show plots of the cumulative rotational angle of the two previous gears. **g** shows the setup to fix the gears onto the surface. **h** and **j** show snapshots of the particles rotating gears A and B, which are fixed to the center of the surface. The pictures also indicate the direction of rotation. **i** and **k** show plots of the cumulative rotational angle of the two fixed gears.

4.4 Sorting of Chiral Active Particles

In this section we show how to sort chiral active particles based only on the orientation of their trajectories. As explained in section 4.2, chirality has two types of orientation: clockwise (dextrogyre) and counter-clockwise (levogyre) [3]. However, regardless of the trajectory, chiral particles displace randomly in a homogeneous environment, such as their non-chiral counterparts.

As shown in the previous experiments, we can introduce order into the system by modifying the environment. In this case, the objective is to sort the chiral particles according to the direction of their rotation. To do this, we based on the results obtained by Mijalkov and Volpe in 2013 [3].

In their research, the authors designed a structure called *chiral flower*. A chiral flower is made up of a set of ellipses placed equidistantly along a circumference, resembling "petals". To create a chiral flower, we consider the following parameters:

- Radius of the flower (a)
- Length of the petal (l)
- Width of the petal (w)
- Angle between the petal and the radius (ξ)

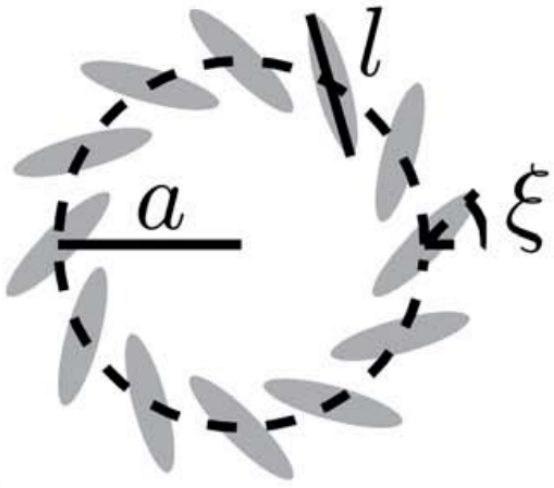

Figure 4.8: Simulation of a Chiral Flower. Image Obtained From [3].

For this experiment we created two chiral flowers that are the mirror inverse of each other. To do this, we 3D-printed the petals: 12 blue ellipses and 12 yellow ellipses. The parameters chosen for the petals were:

- a = 10 cm
- l = 9 cm
- w = 0.9 cm
- $\xi = \pm 60°$.

FIG. 4.9a shows the chiral flowers used for this experiment. We built the set up as follows:

1. We used the boundary shown in FIG. 3.3 to confine an area on a smooth table.
2. We assembled the two chiral flowers within the boundary
3. We modified two HEXBUGS to show dextrogyre chirality, such as in FIG 4.2d.
4. We modified two HEXBUGS to show levogyre chirality, such as in FIG 4.2g.
5. We stuck a bright-colored tags on a HEXBUG for tracking purposes. The colors differed between dextrogyre and levogyre particles.
6. We put the HEXBUGS within the boundary and allowed them to move freely.

We ran the experiment for approximately 1000 seconds. FIG. 4.9a shows a snapshot of the trajectories of the HEXBUGS at a specific time. As illustrated, each flower captures a group of chiral particles depending on the orientation of their rotation.

Using OpenCV, we tracked the positions of the particles throughout the video and counted how many times the particles were inside a flower. FIG. 4.9b shows a bar diagram with the totality of the counts. The orange-colored bars represent the levogyre HEXBUGS, while the purple-colored bars represent the dextrogyre HEXBUGS.

As shown, the levogyre HEXBUGS were found in the left flower seven times more frequently than the dextrogyre particles. This happens because, when levogyre bugs enter the flower, they constantly collide with the petals in the border. The orientation of the petals deviates the levogyre trajectories to the inner parts of the flower. In contrast, when dextrogyre bugs enter the flower and collide with the petals, their trajectory is deviated to the outer parts of the flower. For this reason, the levogyre HEXBUGS remain trapped for longer times, while the dextrogyre bugs escape quickly.

Within the right flower, the dextrogyre HEXBUGS were found two times more frequently than their levogyre counterparts. This occurs for the same reason described for the left flower, due to the symmetry of the experiment.

These results demonstrate that using the chiral flowers, we can effectively sort the particles by their chirality. The observations agree with the results shown by Mijalkov and Volpe. However, the experimental set up is less efficient that the simulations.

Figure 4.9c-e show a series of snapshots of the motion of a dextrogyre HEXBUG. As shown, the bug remains trapped within the flower until another particle interrupts its trajectory and pushes it out of the flower. This happened frequently because of the limited space of the boundaries.

Additionally, the size of the particles also influences this behavior, because they are big in comparison to the size of the right flower. For this reason, the space between the petals must be wider than in the simulation, allowing the HEXBUGS to escape more frequently.

This also happened in the left flowers with the levogyre particles, although to less extents. Nonetheless, the data shows that the experiment is coherent with the theory and further work could produce more accurate results.

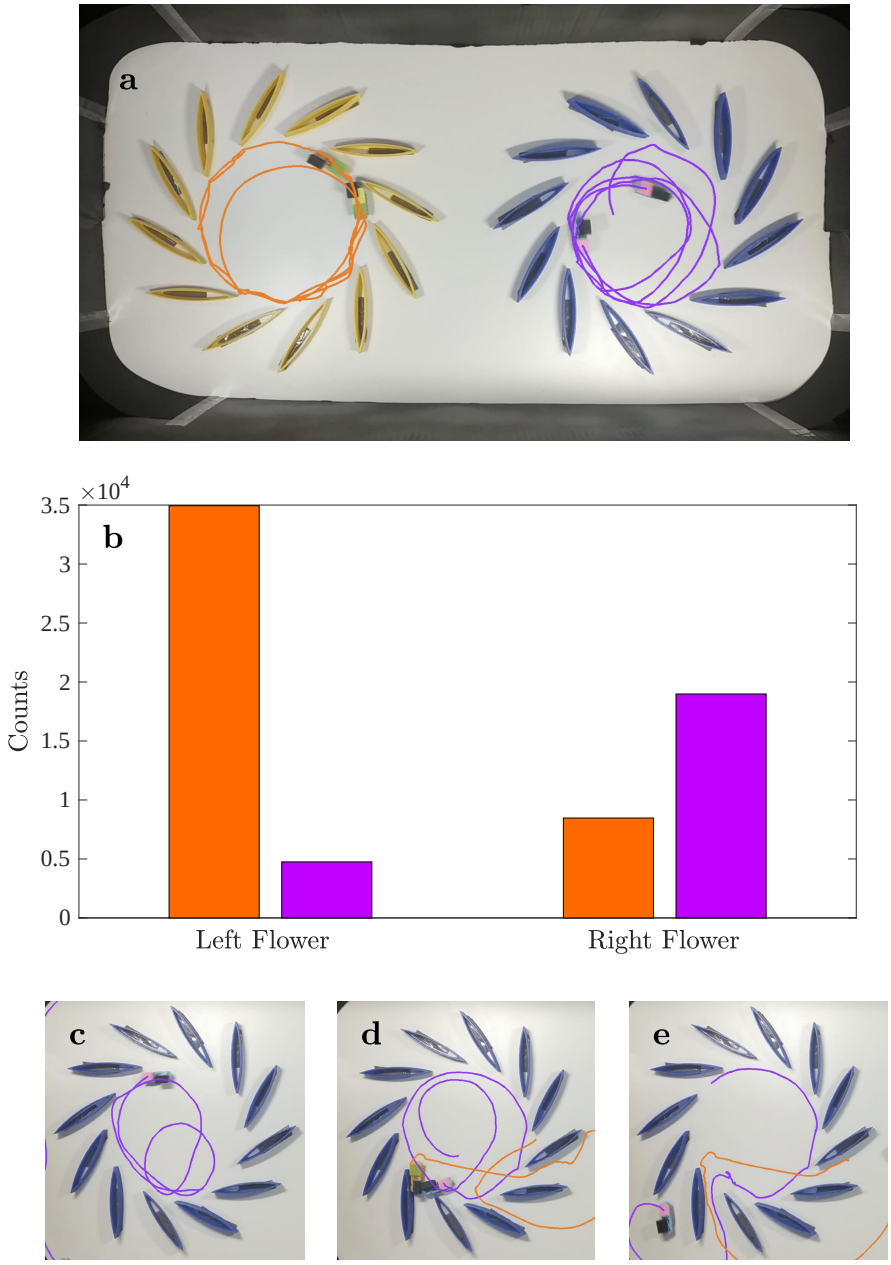

Figure 4.9: Distribution of chiral active particles in chiral traps. **a** shows a snapshot of chiral active particles within dextrogyre and levogyre chiral traps respectively. **b** and **c** shows a histogram of the spatial distribution of dextrogyre and levogyre particles respectively.

4.5 Attractive Forces on Rods

This experiment is based on a paper by Reichhardt et al. (2014) [11]. Their research shows how active matter creates attractive forces between two parallel plates.

Unlike the experiments in section 4.3, these plates do not have concave corners that rectify motion. In this case, the random motion of the active particles creates density fluctuations within the boundaries. Eventually, the region in between the two plates empties and the plates come together. This is called the Casimir effect. FIG. 4.10

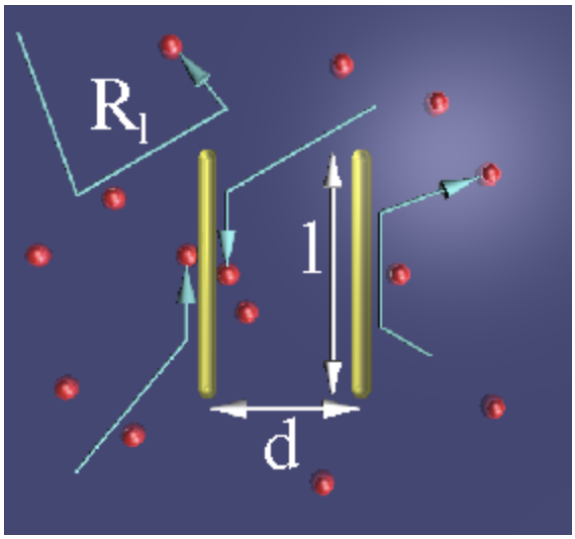

Figure 4.10: Schematic of the Casimir Effect. Image Obtained From [11].

In the simulations by Reichhardt et al., the researchers fixed two walls within a box. To analyze the results, they measured the density of the particles in all the regions in the box, as well as the forces that the particles exert on the walls.

In our experimental version, we assembled two parallel rods using the same 3D-printed cylinders as in sections 4.3. We let the rods loose, therefore, we expected them to come close together.

For this experiment, the two symmetric rods had a size of 2×18 cm. We used 14 HEXBUGS and set up the experiment as follows:

1. We used the boundary shown in FIG. 3.2 to confine an area on a smooth table.
2. We stuck a long bright-colored tag on each of the rods. Each tag had a different color.
3. We placed the rods parallelly within the area at a distance of 15 cm from each other.

4. We homogeneously distributed the HEXBUGS within the boundary and allowed them to move freely.

We analyzed the results by measuring the area of separation in between the two rods. To define the area of separation $A(t)$, we used OpenCV to identify four corners: the two right corners of the leftmost rod and the two left corners of the rightmost rod. By doing this, we obtain a polygon with a specific area.

The area $A(t)$ of the polygon changes according to the separation between the rods. To calculate $A(t)$ we use the **shoelace formula**, which is as follows:

$$A = \frac{1}{2}\left|\sum_{i=1}^{n}(x_i y_{i+1} - x_{i+1} y_i)\right| \tag{4.5}$$

where x_n and y_n are the cartesian coordinates of the polygon, listed in clockwise order [17].

FIG. 4.11a shows snapshots of the trajectory of the two rods at specific times. The snapshots demonstrate that the two parallel rods eventually come together. FIG. 4.11b shows a plot of the area as a function of time $A(t)$. We observe that the area becomes 0 at $t \approx 120$ s. Subsequently, $A(t)$ continues oscillating around low values for the rest of the experiment.

This behavior is expected because the area in between the rods is smaller in comparison to the area that surrounds it. Due to the diffusive nature of Brownian motion, the probability of finding particles in the bigger area is higher. This means that when they collide with the rods, they push the rods towards the inner side of the boundaries, reducing the area between them.

Also, FIG. 4.11b shows an orange solid line. This line represents the area of separation when the width is the size of a HEXBUG, $A(t) = w_{HEXBUG} \times h_{rod} = 1.7$ cm $\times$ 18 cm $= 30.6$ cm. As shown, the oscillations in the area grow approximately to the level of this orange line. This is because the variation in $A(t)$ is caused by the HEXBUGS occasionally opening a path in between the rods.

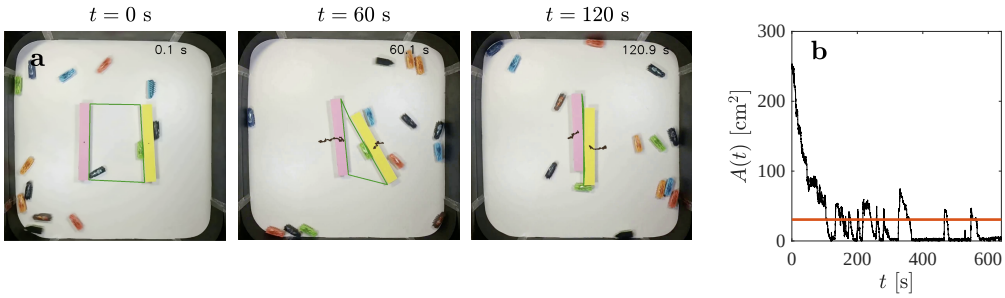

Figure 4.11: Attractive forces using active Brownian particles. **a** shows snapshots of two parallel rods being displaced towards each other. **b** shows a how the area between the two rods varies in time.

5

Conclusion

In this project we accomplished the following:

1. Demonstrate that the HEXBUGS emulate the behavior of active particles.
2. Use the HEXBUGS to produce macroscopic recreations of experiments related to active matter.
3. Ensure that the recreations are simple, understandable, and replicable.

In our first two experiments, we analyzed the behavior of the HEXBUG robots and evaluated its motion patterns. After recording and analyzing its trajectory, we concluded that a HEXBUG, without any modification, moves like an active Brownian particle with limited chirality. Furthermore, we observed that by modifying the weight distribution of the HEXBUGS, they exhibit chiral motion as well.

Based on this information, we used HEXBUGS to replicate simulations of microscopic active matter in a macroscopic scale. Using simple setups, we recreated the scenarios described in several simulation cases. Despite some differences and limitations, the setups we elaborated were accurate enough to produce results that were similar to the theory.

Using computer vision tools we analyzed our experiments and concluded that the behaviors exhibited in simulations were reproducible in real life. These results could be very helpful for didactic applications in the future. Students and researchers would greatly benefit from creating toy models to test some rather abstract theories of non-equilibrium dynamics.

In spite of the good results, this project also had some complications. Further work could address the following issues:

- The HEXBUGS frequently get stuck in the spaces in between the barriers.
- The HEXBUGS often fall on their side and cannot get up.
- HEXBUGS interfere in each others trajectory very frequently.

- It is difficult to film in a larger arena.

Although none of these issues is fatal, improving on them would benefit the quality of the results.

Bibliography

[1] Di Leonardo, R., Angelani, L., Dell'Arciprete, D., Ruocco, G., Iebba, V., Schippa, S., Conte, M., Mecarini, F., De Angelis, F. and Di Fabrizio, E., 2010. Bacterial ratchet motors. Proceedings of the National Academy of Sciences, [online] 107(21), pp.9541-9545. Available at: <https://www.pnas.org/doi/epdf/10.1073/pnas.0910426107> [Accessed 23 June 2022].

[2] Yeomans, J., 2017. Nature's engines: active matter. Europhysics News, [online] 48(2), pp.21-25. Available at: <https://www.europhysicsnews.org/articles/epn/abs/2017/02/epn2017482p21/epn2017482p21.html> [Accessed 1 June 2022].

[3] Mijalkov, M. and Volpe, G., 2013. Sorting of chiral microswimmers. Soft Matter, [online] 9(28), p.6376. Available at: <https://pubs.rsc.org/en/content/articlepdf/2013/sm/c3sm27923e> [Accessed 1 June 2022].

[4] Volpe, G., Gigan, S., Volpe, G. (2014). Simulation of the active Brownian motion of a microswimmer. American Journal of Physics, 82(7), 659–664. doi:10.1119/1.4870398

[5] Leoni, M., Paoluzzi, M., Eldeen, S., Estrada, A., Nguyen, L., Alexandrescu, M., Sherb, K. and Ahmed, W., 2020. Surfing and crawling macroscopic active particles under strong confinement: Inertial dynamics. Physical Review Research, [online] 2(4). Available at: <https://journals.aps.org/prresearch/pdf/10.1103/PhysRevResearch.2.043299> [Accessed 1 June 2022].

[6] Sprenger, A. R., Fernandez-Rodriguez, M. A., Alvarez, L., Isa, L., Wittkowski, R., Loewen, H. (2020). Active Brownian motion with orientation-dependent motility: theory and experiments. Langmuir. doi:10.1021/acs.langmuir.9b03617

[7] Wan, M., Olson Reichhardt, C., Nussinov, Z. and Reichhardt, C., 2008. Rectification of Swimming Bacteria and Self-Driven Particle Systems by Arrays of Asymmetric Barriers. Physical Review Letters, [online] 101(1). Available at: <https://journals.aps.org/prl/abstract/10.1103/PhysRevLett.101.018102> [Accessed 1 June 2022].

[8] Wang, J. and Gao, W., 2012. Nano/Microscale Motors: Biomedical Opportunities and Challenges. ACS Nano, [online] 6(7), pp.5745-5751. Available at: <https://pubs.acs.org/doi/10.1021/nn3028997> [Accessed 1 June 2022].

[9] Bechinger, C., Di Leonardo, R., Löwen, H., Reichhardt, C., Volpe, G. and Volpe, G., 2016. Active Particles in Complex and Crowded Environments. Reviews of Modern Physics, [online] 88(4). Available at: <https://www.researchgate.net/publication/301856934_Active_Particles_in_Complex_and_Crowded_Environments> [Accessed 1 June 2022].

[10] Angelani, L. and Leonardo, R., 2010. Geometrically biased random walks in bacteria-driven micro-shuttles. New Journal of Physics, [online] 12(11), p.113017. Available at: <https://iopscience.iop.org/article/10.1088/1367-2630/12/11/113017/pdf> [Accessed 1 June 2022].

[11] Ray, D., Reichhardt, C. and Reichhardt, C., 2014. Casimir effect in active matter systems. Physical Review E, [online] 90(1). Available at: <https://journals.aps.org/pre/abstract/10.1103/PhysRevE.90.013019> [Accessed 1 June 2022].

[12] Soft Active Matter Lab. 2022. Research. [online] Available at: <https://activematterlab.org/research/#:~:text=Inspired%20by%20several%20active%20microscopic,%2Ddelivery%2C%20and%20gene%20therapy> [Accessed 1 June 2022].

[13] Khadka, U., Holubec, V., Yang, H. et al. Active particles bound by information flows. Nat Commun 9, 3864 (2018). https://doi.org/10.1038/s41467-018-06445-1

[14] Hexbug.com. 2022. HEXBUG nano® 5 Pack - 4 nano Plus Bonus Flash Nano®. [online] Available at: <https://www.hexbug.com/hexbug-nano-5-pack-4-nano-plus-bonus-flash-nano.html#additional> [Accessed 29 June 2022].

[15] Mi.com. 2022. Mi Global Home. [online] Available at: <https://www.mi.com/global/redmi-s2> [Accessed 1 June 2022].

[16] Docs.opencv.org. 2022. OpenCV: Introduction. [online] Available at: <https://docs.opencv.org/4.6.0/d1/dfb/intro.html> [Accessed 1 June 2022].

[17] R. Ochilbek, "A New Approach (Extra Vertex) and Generalization of Shoelace Algorithm Usage in Convex Polygon (Point-in-Polygon)," 2018 14th International Conference on Electronics Computer and Computation (ICECCO), 2018, pp. 206-212, doi: 10.1109/ICECCO.2018.8634725.

DEPARTMENT OF APPLIED PHYSICS
CHALMERS UNIVERSITY OF TECHNOLOGY
Gothenburg, Sweden
www.chalmers.se

CHALMERS
UNIVERSITY OF TECHNOLOGY